

System-level simulation of liquid filling in microfluidic chips

Hongjun Song, Yi Wang,^{a)} and Kapil Pant
CFD Research Corporation, Huntsville, Alabama 35805, USA

(Received 23 February 2011; accepted 20 April 2011; published online 19 May 2011)

Liquid filling in microfluidic channels is a complex process that depends on a variety of geometric, operating, and material parameters such as microchannel geometry, flow velocity/pressure, liquid surface tension, and contact angle of channel surface. Accurate analysis of the filling process can provide key insights into the filling time, air bubble trapping, and dead zone formation, and help evaluate trade-offs among the various design parameters and lead to optimal chip design. However, efficient modeling of liquid filling in complex microfluidic networks continues to be a significant challenge. High-fidelity computational methods, such as the volume of fluid method, are prohibitively expensive from a computational standpoint. Analytical models, on the other hand, are primarily applicable to idealized geometries and, hence, are unable to accurately capture chip level behavior of complex microfluidic systems. This paper presents a parametrized dynamic model for the system-level analysis of liquid filling in three-dimensional (3D) microfluidic networks. In our approach, a complex microfluidic network is deconstructed into a set of commonly used components, such as reservoirs, microchannels, and junctions. The components are then assembled according to their spatial layout and operating rationale to achieve a rapid system-level model. A dynamic model based on the transient momentum equation is developed to track the liquid front in the microchannels. The principle of mass conservation at the junction is used to link the fluidic parameters in the microchannels emanating from the junction. Assembly of these component models yields a set of differential and algebraic equations, which upon integration provides temporal information of the liquid filling process, particularly liquid front propagation (i.e., the arrival time). The models are used to simulate the transient liquid filling process in a variety of microfluidic constructs and in a multiplexer, representing a complex microfluidic network. The accuracy (relative error less than 7%) and orders-of-magnitude speedup (30 000X–4 000 000X) of our system-level models are verified by comparison against 3D high-fidelity numerical studies. Our findings clearly establish the utility of our models and simulation methodology for fast, reliable analysis of liquid filling to guide the design optimization of complex microfluidic networks. © 2011 American Institute of Physics. [doi:10.1063/1.3589843]

I. INTRODUCTION

Lab-on-a-chip (LoC) systems are miniaturized devices to achieve multiplexed analysis by integrating various components, such as injection, mixing, reaction, separation, detection on a microchip platform, and have found a variety of applications in biology, medicine, and chemistry.^{1,2} In contrast to the traditional analytical techniques, the LoC system has many advantages, such as reduced usage of reagents and samples, fast analysis time, and high-level integration and automation.

^{a)}Tel.: 256-327-0678. Electronic mail: yxw@cfdr.com.

Precise injection and filling of the liquid samples and reagents into a microfluidic network for desired analysis is a complex process that depends on a variety of geometric, operating, and material parameters, such as microchannel geometry, flow velocity/pressure, liquid surface tension, and contact angle of channel surface.³ Variations in these parameters can result in distinctly different filling behavior in terms of filling time, air bubble trapping, and dead zone formation.⁴ Investigation of liquid filling process can guide protocol development and layout design to avoid potential filling problems.⁵

Liquid filling process has been widely investigated, primarily for a single microfluidic component or capillary. Kim *et al.*⁶ experimentally and numerically investigated transient liquid filling into microchannels by considering the surface tension effect. The results indicate that surface tension significantly affects the filling flow; even flow blockage was observed at channels of small cross section. Tseng *et al.*⁷ investigated fluid filling into microreservoirs. The filling process was demonstrated experimentally using microparticle image velocimetry and also validated by numerical simulation. The capillary filling dynamics in centrifugally actuated microfluidic platforms with dynamically evolving contact line motion was analyzed by Chakraborty *et al.*⁸ The prediction of liquid filling process using both semianalytical approach and fully numerical approach was found to be in good agreement with the experimental data. An analytical model based on momentum conservation was developed by Zeng⁵ for liquid filling in two-dimensional (2D) straight channels, and a good agreement was obtained between the numerical analysis and the analytical model. However, single-component models are unable to capture the geometric, topological, and material property effects in the complex microfluidic network at the system level and, hence, inadequate, for chip design and optimization. Ahn *et al.*^{9–11} presented a structurally programmable microfluidic system to passively controlled flow, which is accomplished by adjusting the unequal dimension in channel width and length. An analytical expression was used to predict the pressure drop across a liquid plug, which, however, cannot be used to assess the filling time.⁹ On the other hand, high-fidelity numerical methods (e.g., volume of fluid or level set) have been widely used to investigate the complex filling behavior in microfluidic networks.^{4,12} Despite their salient accuracy, numerical methods are prohibitively expensive, leading to long analysis time (several hours to several days).

To overcome these limitations, reduced order models have been introduced for rapid system-level analysis and design of LoC devices.^{13–15} Treise *et al.*¹⁶ used a constrained energy minimization approach for modeling liquid filling in microfluidic components and networks. The computational time was reduced to several minutes and the results matched the experimental data well in terms of the liquid front face profile and flow volume for a variety of single components and small networks. However, due to the lack of fluid dynamic considerations, this model cannot predict the speed and time of the liquid filling in the network that are critical from a chip design perspective.

To address the aforementioned issues, this paper presents a parametrized dynamic model for the system-level analysis of liquid filling in three-dimensional (3D) microfluidic networks. In our approach, a complex microfluidic network is deconstructed into a set of commonly used components, such as reservoirs, microchannels, and junctions. The components are then assembled according to their spatial layouts and operating rationale to achieve a rapid system-level model. The dynamic model based on the transient momentum equation is developed to track the liquid filling front in the microchannel component. The principle of mass conservation at the junction is used to link the fluidic parameters in the microchannels emanating from the junction. Assembly of these component models yields a set of differential and algebraic equations (DAEs), which upon integration provides temporal information of the liquid filling process, such as the pressure distribution and liquid front propagation (i.e., the arrival time). This paper is organized as follows: first, we present the system-level representation of the microfluidic network in Sec. II. A description of the component models is given in Sec. III and the systematic model is presented in Sec. IV. The transient liquid filling process in a variety of microfluidic constructs (including Y-junctions with various branch angles, branch channel sizes, and contact angles) and in a complex microfluidic

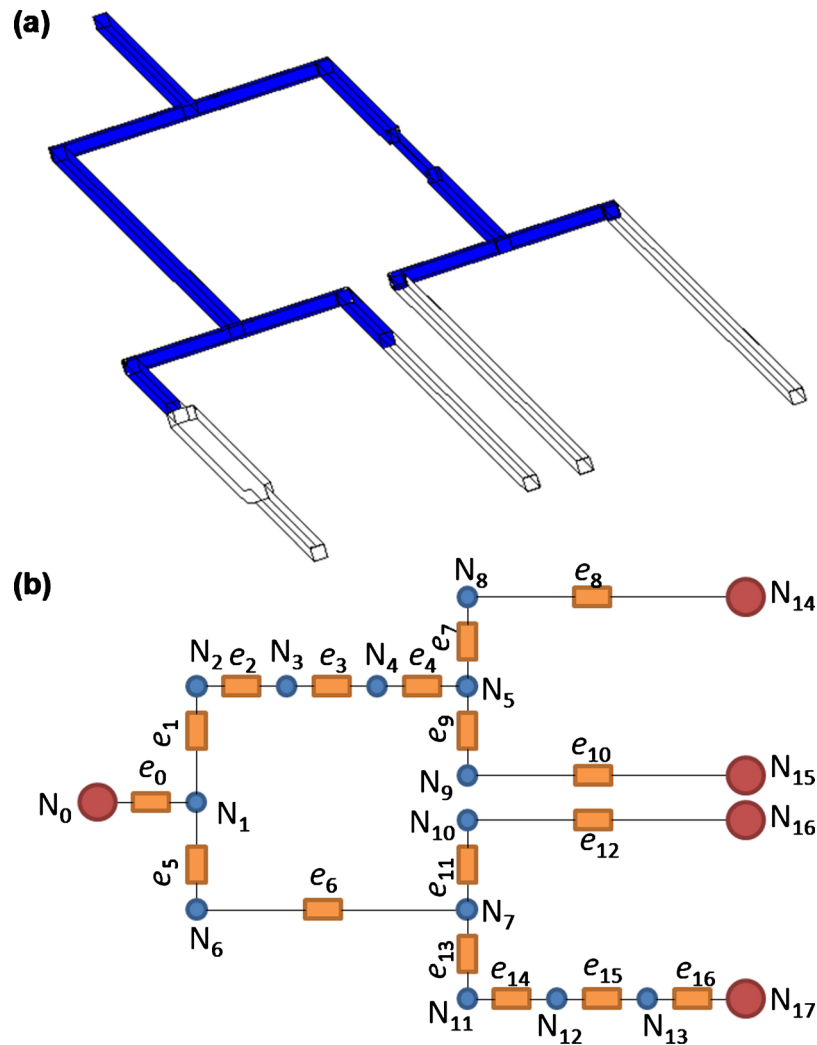


FIG. 1. A complex microfluidic multiplexer: (a) the physical model and (b) the system-level model.

network (multiplexer) is analyzed in Sec. V. The simulation results are validated by comparing against 3D high-fidelity numerical studies using CFD-ACE+. A summary and possible future work is concluded in Sec. VI.

II. SYSTEM-LEVEL REPRESENTATION

Figure 1 illustrates the schematic representation of our system-level simulation. A microfluidic network is composed of a network of connected components. Each component is denoted by an edge (e_i), which corresponds to a microchannel. Components are connected via junctions, which are represented by nodes (N_i) in Fig. 1. Each edge has its own geometric parameters (such as length, width, and height) and surface properties (such as the contact angle). Each node is treated as a pointwise connection between the upstream and the downstream edges. The inlet and outlet are also treated as special nodes, which are only connected to the downstream edge or the upstream edge, respectively. For example, the microfluidic multiplexer in Fig. 1(a) consists of 17 edges (e_0 – e_{16}) and 18 nodes (N_0 – N_{17}), as shown in Fig. 1(b). Such a decomposable approach enables the development of parametrized models for each component that can be reused to represent chip designs of various topologies, geometries, and material properties.

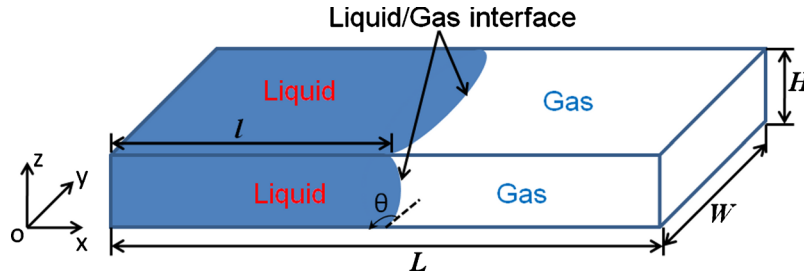


FIG. 2. The physical model of a microchannel.

III. COMPONENT MODELS

In this section, the governing equations and component models of microchannels and junctions for liquid filling are presented.

A. Microchannels

Figure 2 illustrates the coordinate system and notations in a straight channel (i.e., edge), where x , y , and z represent axial, widthwise, and depthwise coordinates, and L , W , and H denote the length, the width, and the height of the channel, respectively. The contact angle between the solid surface and the liquid is θ . l is the filled length in the channel. The following assumptions are made to simplify the models:

- (1) The flow is fully developed (neglecting the entry region at the channel inlet).
- (2) The flow is laminar and the assumption of the quasisteady state,¹² featuring a low Reynolds number (typically $\ll 100$).
- (3) The formation and transportation of trapped air plugs in the microfluidic networks are not accounted for.

The filling status of a microchannel can be classified into three categories: (1) void (no liquid in the channel, $l=0$), (2) partially filled (partial liquid and partial gas, $l < L$), and (3) fully filled (all liquid, $l=L$). For the void cases, there is no liquid inside the channel, and hence the pressure at the inlet and at the outlet is equal to

$$P_{\text{in}} - P_{\text{out}} = 0, \quad (1)$$

where P_{in} and P_{out} is the pressure at the inlet and outlet of the channel, respectively.

For the fully filled cases, the flow within the channel is governed by

$$\frac{\partial^2 u}{\partial y^2} + \frac{\partial^2 u}{\partial z^2} = -\frac{1}{\mu} \frac{\partial P}{\partial x}, \quad (2)$$

where μ is the dynamic viscosity and u is the axial velocity of the liquid. For fully developed flow [i.e., $\partial P / \partial x = (P_{\text{in}} - P_{\text{out}}) / L$], Eq. (2) can be solved analytically¹⁷ yielding the following balance equation:

$$\frac{12\beta L \mu Q}{W^4 \gamma} - (P_{\text{in}} - P_{\text{out}}) = 0, \quad (3)$$

where $Q = \int_0^H \int_0^W u dy dz$ is the flow rate, $\beta = W/H$ is the aspect ratio of the channel, and $\gamma = 1 - (192\beta) \sum_{i=1,3,5,\dots}^{\infty} \tanh(i\pi/2\beta) / (i\pi)^5$. Thus, the cross-sectional average flow velocity, $U = \beta Q / W^2$, can be obtained by rewriting Eq. (3) as

TABLE I. Liquid filling length and the force balance equation for each filling status.

Filling status	Liquid length (l)	Balance equation
Void	$l=0$	$P_{\text{in}}-P_{\text{out}}=0$
Partially filled	$0 < l < L$	$2\sigma \cos \theta(1+\beta) + (P_{\text{in}}-P_{\text{out}})W - 12\mu l / W\gamma dl/dt = 0$
Fully filled	$l=L$	$12\mu L / W\gamma U - (P_{\text{in}}-P_{\text{out}})W = 0$

$$\frac{12\mu L}{W\gamma}U - (P_{\text{in}} - P_{\text{out}})W = 0, \quad (4)$$

In the partially filled case, there is a liquid-gas interface within the channel, and the momentum of the associated liquid plug can be written as $\rho HWlU$. Based on the Newton's second law, the momentum change is balanced by surface tension force, pressure difference, and viscous force, which is expressed as

$$\frac{d(\rho HWlU)}{dt} = 2\sigma \cos \theta(1 + \beta) + (P_{\text{in}} - P_{\text{out}})W - \frac{12\mu l}{W\gamma}U, \quad (5)$$

where σ is the surface tension coefficient, θ is the contact angle, and l is the filling length within the channel (as shown in Fig. 2). Based on the quasisteady state assumption, the momentum change in Eq. (5), i.e., LHS, is negligible. Thus, the force balance equation can be recast as

$$2\sigma \cos \theta(1 + \beta) + (P_{\text{in}} - P_{\text{out}})W - \frac{12\mu l}{W\gamma} \frac{dl}{dt} = 0, \quad (6)$$

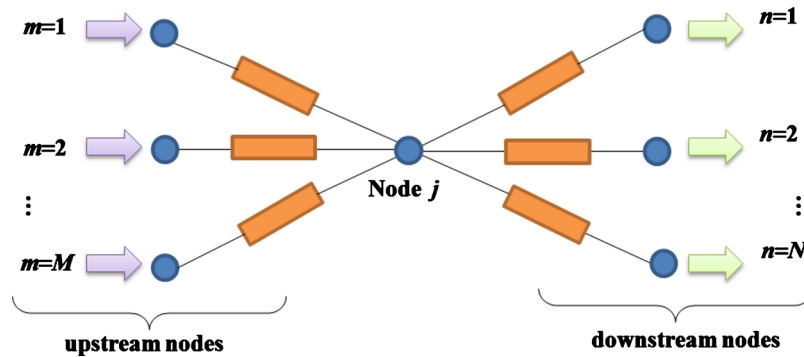
where $U=dl/dt$ is substituted into the equation. Note that P_{in} and P_{out} in Eq. (6) are the liquid pressure at the inlet and the air pressure at the outlet of the channel, respectively. The time-varying filling length l can be obtained by integrating the ordinary differential equation (ODE) in Eq. (6). The liquid plug length within the channel and the force balance equation for each filling status are summarized in Table I.

B. Junctions

In our system-level representation, junctions are represented by nodes and can have two filling status: void or filled. In the void case, the junction is not filled and its pressure remains the same as the ambient pressure. In the filled case, the junction is soaked and the principle of mass conservation at the junction can be used to link the flow rates through the edges emanating from the junction, which for a node j is given by

$$\sum_{m=1}^M Q_m^j - \sum_{n=1}^N Q_n^j = 0, \quad (7)$$

where $j=1,2,\dots,J$ and J is the total number of nodes in the network, m is the index of the upstream edges of node j , $m=1,2,\dots,M$, and M is the total number of upstream edges. Likewise, n is the index of the downstream edges of node j , $n=1,2,\dots,N$, and N is the total number of upstream nodes. Thus, $\sum_{m=1}^M Q_m^j$ and $\sum_{n=1}^N Q_n^j$ are the total flow rates entering and exiting node j , respectively. A schematic of the connection of node j is shown in Fig. 3. Note that as the trapping of the air bubble is not taken into account, the current model particularly handles the case with $M=1$ (e.g., multiplexer-type network). The more general scenario that involves multiple upstream edges (i.e., $M>1$) linked to a single node and can potentially cause bubble formation will be addressed in the future effort.

FIG. 3. The schematic of the connection of node j .

IV. SYSTEM-LEVEL MODEL

We now integrate the aforementioned component models to obtain a system model for simulating the liquid filling process. The simulation involves computing fluidic parameters, including pressure (P) and flow rates (Q), and tracking the liquid-air fronts (i.e., the filled channel length l in Table I and the propagation time t) in the network simultaneously.

The flow rate Q through each edge depends on the pressure difference across it. Thus, Eq. (7) can be rewritten to correlate the flow rate Q^j emanating from node j and the pressure in its neighboring edges m and n (i.e., P_m^{in} , P_m^{out} , P_n^{in} , and P_n^{out}) using the functional relationship in Table I, where “in” and “out” denote the inlet and outlet of the edge.

Fluidic parameters and filling time at the outlet of the upstream edge is set equal to that at the inlet of the downstream edge via node j , i.e., $P_m^{\text{out}} = P_n^{\text{in}} = P^j(t)$ and $t_m^{\text{out}} = t_n^{\text{in}} = t^j$ because of continuity requirements, where P^j and t^j are the pressure and arrival time of the liquid front at node j . Note that P^j depends on time. Equation (7) is applied to each node, yielding a set of algebraic equations for the network. Given the pressure/flow rate at the inlet/outlet as the boundary conditions and the initial filling length $l=0$ as the initial condition, the filling length l in each edge is calculated by integrating Eq. (6). With updated filling length l , the algebraic equation (7) is used to explicitly determine the nodal pressures in the network. These two steps are then recursively iterated in the temporal integration to track the propagation of all liquid fronts in the network. The software library CVODE (<http://www.llnl.gov/CASC/sundials/>) and SuperLU (<http://crd.lbl.gov/~xiaoye/SuperLU/>) are adopted, respectively, for integrating the ODE equations governing the filling length and solving the set of algebraic equations of the pressures in the network. In particular, an internal linear solver of CVODE, CVDENSE, was used for ODE integration by Newton iteration scheme. In all simulations, the tolerance of the relative error and the absolute error is 1.0×10^{-06} and 1.0×10^{-20} , respectively.

The flow chart of the system-level simulation for liquid filling is shown in Fig. 4. The network topology, geometry and size, and surface properties (e.g., contact angle), boundary conditions (such as inlet velocity/pressure and outlet pressure), and fluid properties (such as density, viscosity, and surface tension coefficient) are read by the solver. The solver then initiates the filling length and pressure of the liquid at each edge and node, followed by the ODE integration for the new filling length at each edge and update of the pressure at each node. This two-step calculation is iterated alternatively until the filling length of the liquid at each edge remains within a specified tolerance. Finally, the filling time and status in each edge/node are updated.

V. RESULTS AND DISCUSSION

In this section, the system-level models are applied to investigate the liquid filling process in a variety of microfluidic constructs (Y-junction with various branch angles, branch channel sizes, and contact angles) and in complex microfluidic networks (splitter and multiplexer). The system-level simulation results are validated against high-fidelity numerical analysis performed with

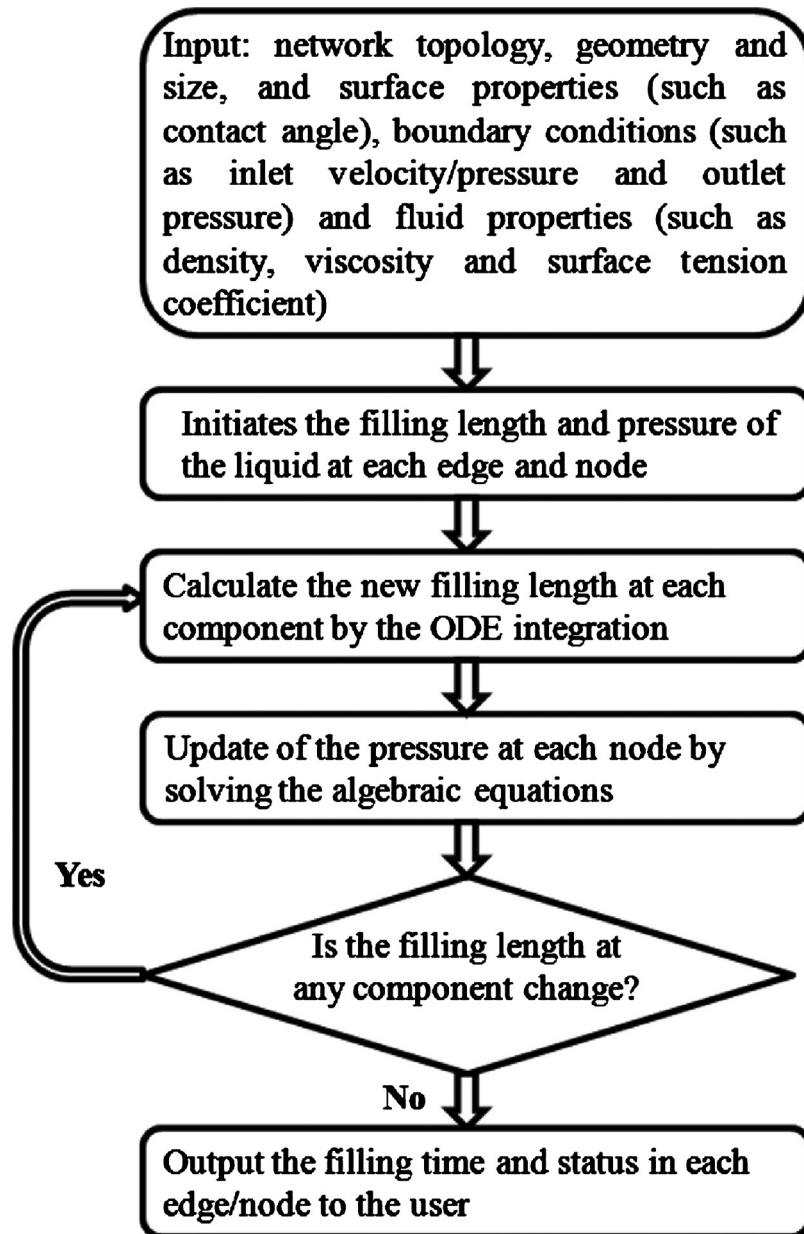


FIG. 4. Flow chart of the system-level model of liquid filling process in microfluidic network.

CFD-ACE+ (ESI-CFD, Inc.), in which the fluidics and volume of fluid (VOF) module are invoked to resolve the multiphase flow and the motion of the liquid/gas interface. As a commercial software package, the VOF module in CFD-ACE+ has been widely validated for liquid filling and droplet evolution in microchannels and chambers by experimental results from various sources.^{18–23} The parameters used in the simulation include the density of the liquid, $\rho = 1000 \text{ kg/m}^3$, the surface tension coefficient, $\sigma = 0.0725 \text{ N/m}$, and the dynamic viscosity of the liquid, $\mu = 8.9 \times 10^{-4} \text{ m}^2/\text{s}$. An automatic adaptive time step approach is used in CFD-ACE+ simulation and a constant small time step size of 0.0005 s is used in the system-level model to ensure high accuracy for all case studies in the paper. The average grid densities in CFD-ACE+ simulation are 20 nodes/mm in the longitudinal direction of the microchannel and 100 nodes/mm in the transverse direction. These node densities were arrived via iterative solutions to ensure

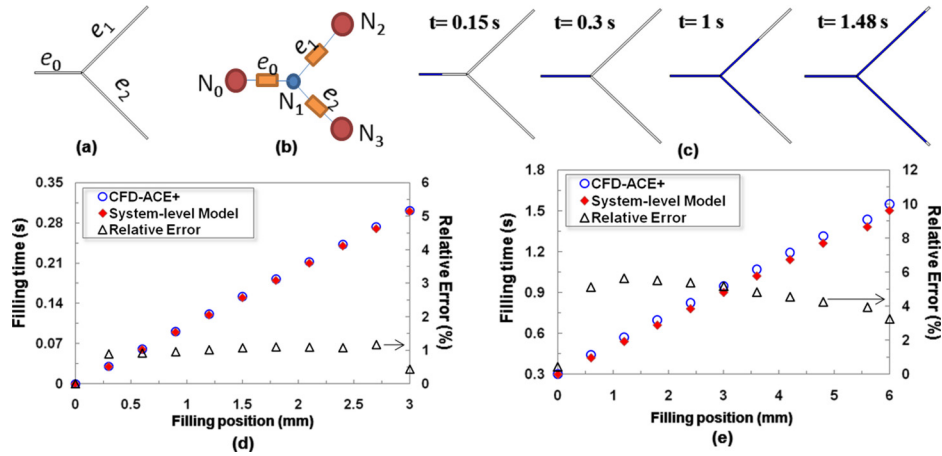


FIG. 5. (a) Schematic of Y-junction with channels of the same width (solid column denotes liquid); (c) a series of snapshots of the liquid filling process at different times; (d) the filling time at different filling positions in edge e_0 and the relative error; and (e) the filling time at different filling positions in edge e_1 and the relative error.

grid-independent results. In addition, fine grids are adapted at the junction regions (with sharply varying cross sections) to accurately capture the evolution of the free liquid surface therein. Both system-level and CFD-ACE+ simulations are performed on a PC platform equipped with AMD Phenom™ II X4 945 Processor (3 GHz, 3 GB of RAM).

A. Liquid filling in Y-junction channels

We first compare our system-level model against CFD-ACE+ results of liquid filling in Y-junction channels. Figure 5(a) illustrates a simple 2D Y-junction containing three channels: main channel e_0 and two branch channels, e_1 and e_2 . Their widths are all $100 \mu\text{m}$, and their lengths are respectively, 3, 6, and 6 mm. The contact angle θ is 110° , and the inlet flow rate is 0.01 m/s . Figure 5(b) illustrates the system-level schematic representation. A series of snapshots of the liquid filling process at different times is shown in Fig. 5(c). The liquid (denoted by the solid column) first marches in the main channel e_0 and then branches out into channel e_1 and e_2 after e_0 is filled. The filling time of e_0 is about 0.3 s and that of e_1 and e_2 are about 1.5 s. Both match well during the filling process. The comparison between the system-level model and the CFD-ACE+ analysis in terms of the filling time and the filling position in e_0 , e_1 is exhibited in Figs. 5(d) and 5(e), respectively. Excellent agreements are observed in all the channels with a relative error of less than 6%. The computational times of our system-level model and CFD-ACE+ are, respectively, 0.39 and 183 600 s, yielding a speedup of about 470 000X. The comparison of the filling process in e_2 (not shown) is the same as in e_1 due to the symmetric branch configurations.

1. Effect of the branch channel width

In this section, both high-fidelity CFD-ACE+ analysis and system-level simulation are carried out to investigate the effects of the branch channel width on the liquid filling time in the Y-junction channel. A Y-junction channel similar to the previous one but with asymmetric branches (i.e., the channel widths of the branch channel e_2 , i.e., W_2 reduced from 100 to 90 and $80 \mu\text{m}$) was used in the case study and compared against the symmetric case. Based on Eq. (6), the liquid filling velocity in the partially filled channel can be rewritten as

$$U = \frac{W^2 \gamma}{12 \mu l} [2 \sigma \cos \theta (1 + \beta) / W + (P_{\text{in}} - P_{\text{out}})]. \quad (8)$$

Equation (8) suggests that the filling velocity U strongly depends on the channel width and contact angle. The liquid can be drawn into the channel only if the filling velocity U is positive, where

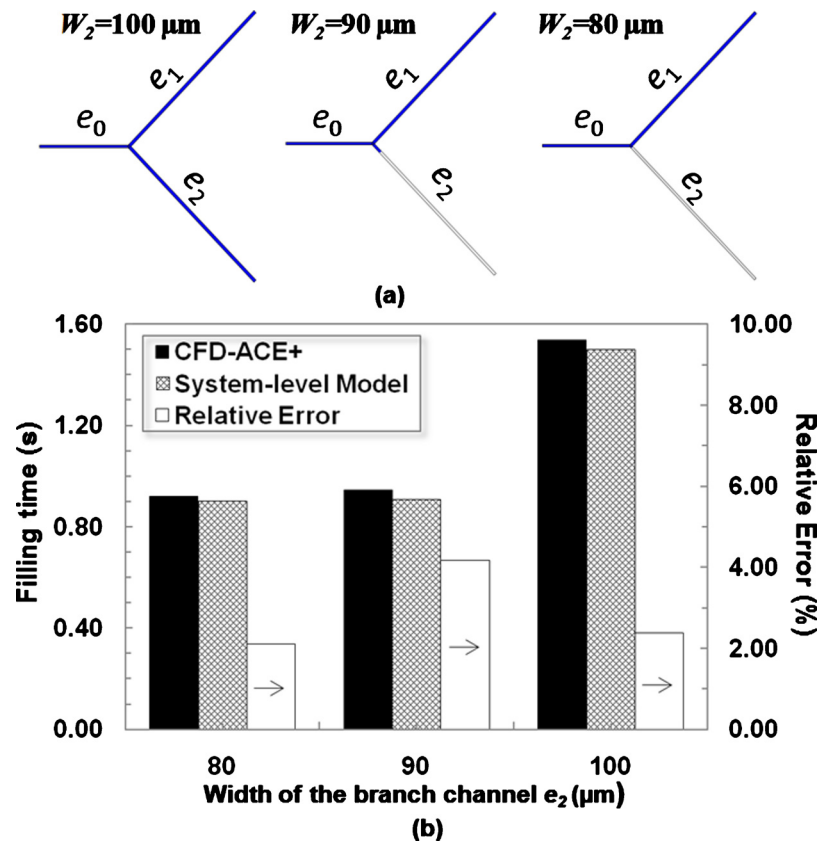


FIG. 6. Effect of the branch channel width: (a) snapshots of the asymmetric filling process in the branch channels with different widths and (b) the filling time when channel e_1 is fully filled.

$2\sigma \cos \theta(1+\beta)/W$ is the surface tension-induced pressure difference and $P_{\text{in}} - P_{\text{out}}$ is the hydrodynamic pressure difference across the channel. The snapshots in Fig. 6(a) exhibit an asymmetric filling process in the branch channels e_1 and e_2 due to their unequal widths. Since the channel walls are hydrophobic (i.e., contact angle $\theta = 110^\circ$), the surface tension acts as a resistive force to liquid filling and is scaled up with the use of small channel width according to Eq. (8). Therefore, the narrower branch channel e_2 is filled at extremely slow rate [e.g., $W_2 = 90 \mu\text{m}$ in the middle of Fig. 6(a)] or cannot be filled at all [e.g., $W_2 = 80 \mu\text{m}$ in the right of Fig. 6(a)]. Figure 6(b) shows the effect of branch channel width W_2 on the filling time of the branch channel e_1 (i.e., the time when channel e_1 is fully filled). As W_2 decreases, the filling time of channel e_1 is significantly shortened (faster filling speed) because most of the liquid is diverted to e_1 . The CFD-ACE+ and system-level simulations match very well with a relative error of less than 5%. Both analyses clearly reveal that unequal branch channel widths result in asymmetric filling and elongated filling time or even filling failure in the worst case.

Upon verification of our system-level model, it is then used to investigate the effect of the asymmetry of the branch channels on the filling velocity in a broader parameter space owing to its fast simulation speed. Figure 7 shows the variation of U_2/U_1 (the ratio of the liquid filling velocity in the branch channels e_1 and e_2) with the filling length in e_1 for different width ratios W_2/W_1 . When both channels have the same width, the liquid in both moves at the same speed (i.e., a symmetric filling process and indicated by the horizontal line with $U_2/U_1 = 1$). With a narrow branch channel e_2 ($W_2/W_1 < 1$), the initial filling velocity U_2 in e_2 is zero and liquid first fills channel e_1 , leading to an asymmetric filling process. Liquid can only start to fill e_2 after e_1 is already filled about 1.2, 2.4, and 5.2 mm for $W_2/W_1 = 0.975, 0.95, 0.9$, respectively. Therefore, the

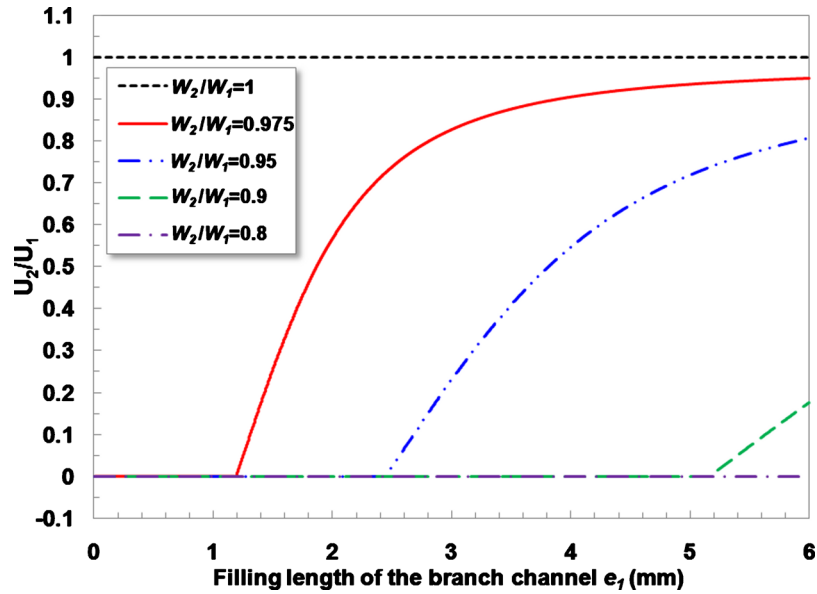


FIG. 7. The relationship of U_1/U_2 and the filling length of branch channel.

liquid filling in e_1 always precedes that in e_2 . No liquid will fill the channel e_2 when W_2/W_1 decreases to 0.8 since U_2 remains zero even when the entire channel e_1 is filled.

2. Effect of the contact angle

In this section, we analyze the effect of the contact angle θ on the liquid filling in the Y-junction channel. In our simulation, two contact angles $\theta=70^\circ$ and $\theta=110^\circ$ were first investigated, and the widths of the branch channel e_1 and e_2 are 100 and 90 μm , respectively. According to Eq. (8), given constant pressure heads $P_{\text{in}}-P_{\text{out}}$ over the branch channels (i.e., $P_{N1}-P_{N2}=P_{N1}-P_{N3}$), the filling velocity and status in them is solely determined by the surface tension force. For $\theta=70^\circ$ (i.e., hydrophilic channel walls), the surface tension aligns with the pressure difference as a driving force to pull the liquid into the channel. As the surface tension is enhanced by the smaller channel width, the liquid preferentially enters the narrower branch channel e_2 at a fast filling speed. The filling into the wider branch channel e_1 is quite slow and significantly delayed [Fig. 8(a)] as a result of the negligible overall driving force at the initial phase. The filling behavior in the hydrophobic microchannels (i.e., $\theta=110^\circ$) is the opposite [Fig. 8(b)]. The liquid first gets into the wider branch channel e_1 , followed by a slow ingress into the narrower channel e_2 . Figures 9(a) and 9(b) show the comparison between the system-level analysis and CFD-ACE+ on the filling time of the nodes for $\theta=70^\circ$ and $\theta=110^\circ$. A worst relative error of less than 7% is observed. The simulation indicates that the liquid is more prone to fill a narrow hydrophilic channel or a wide hydrophobic channel. Therefore, localized surface modification can be utilized for sample manipulation and delivery to the desired regions.

Likewise, the system-level model is used to investigate the effect of the contact angle θ on the asymmetric filling over a wide parameter range. Figure 10 illustrates the filling times of the branch channels e_1 and e_2 (i.e., the arriving times of the liquid front to the outlet nodes N_2 and N_3) for different contact angles. The analysis above indicates that the liquid will first fill e_2 for $\theta<90^\circ$ (hydrophilic), or first fill e_1 for $\theta>90^\circ$ (hydrophobic), which agrees with the observation in Fig. 10 showing that the filling time at N_3 is less than that at N_2 for $\theta<90^\circ$ and longer than that at N_2 for $\theta>90^\circ$. We also note that the filling time at N_3 grows dramatically when θ increases from 90° , and N_3 does not get filled for $\theta>93^\circ$ (given the asymmetric channel ratio $W_2/W_1=0.9$ in this case). This is because for the hydrophobic channel surface, the hydrodynamic pressure drives the liquid through the channel while the surface tension force acts against it. The pressure at N_1 drops

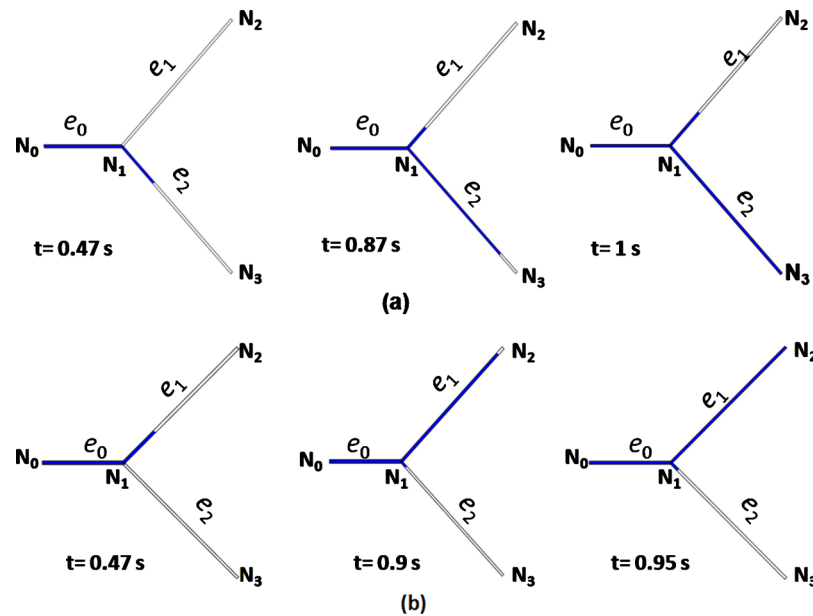


FIG. 8. Snapshots of the asymmetric filling process in the branch channels with different contact angles: (a) $\theta=70^\circ$ (hydrophilic) and (b) $\theta=110^\circ$ (hydrophobic).

once N_2 is filled as the surface tension force in e_1 vanishes, leading to the decrease in the driving force for liquid filling in e_2 . If the reduced driving force is sufficient to overcome the surface tension in e_2 , liquid filling in e_2 will continue but at significantly reduced filling velocity, giving rise to a longer filling time at N_3 (which corresponds to the case for $90^\circ < \theta < 93^\circ$ in Fig. 10). Otherwise, N_3 will never be filled (i.e., the case for $\theta > 93^\circ$). Such incomplete filling (or termed blocking phenomena) has also been experimentally observed by Kim *et al.*,⁶ which further verifies our system-level model.

3. Effect of branch angles

Note that the branch angles of the Y-junction channel are not parametrized in our system-level representation. In this section, high-fidelity numerical analysis is undertaken to investigate the effect of the branch angles on liquid filling and compare against the system simulation results. Y-junction channels with three sets of branch angles are considered, case 1 = $\{135^\circ, 90^\circ, 135^\circ\}$, case 2 = $\{180^\circ, 90^\circ, 90^\circ\}$, and case 3 = $\{90^\circ, 180^\circ, 90^\circ\}$, where the angles in each case are counted starting from the flow inlet in the counterclockwise directions, as illustrated in Fig. 11(a). Note that case 2 and case 3 are essentially T-junction channels. The length and width of all the channels are 400 and 100 μm , respectively. The schematic representation for our system-level analysis is the same in all the three cases due to the lumped feature of the node model (see Fig. 3). Figure 11(b) shows comparison between the CFD-ACE+ analysis and our system-level simulation in terms of the filling time (i.e., the arrival time of the liquid front) at the nodes. Good agreement for all three cases with relative error of less than 5.4% is observed [Fig. 11(c)]. The filling time is virtually the same for all three cases, indicating that the filling process is less susceptible to the branch angles. This confirms that our system-level model is capable of describing the liquid filling process in junction channels with various branch angles. In addition, our system-level model achieves significant speedup over the high-fidelity analysis using CFD-ACE+. It only took the system-level model 0.031 s to run each case in Fig. 11(a), which, however, required at least 20 min using CFD-ACE+, yielding about 38 000-fold speedup.

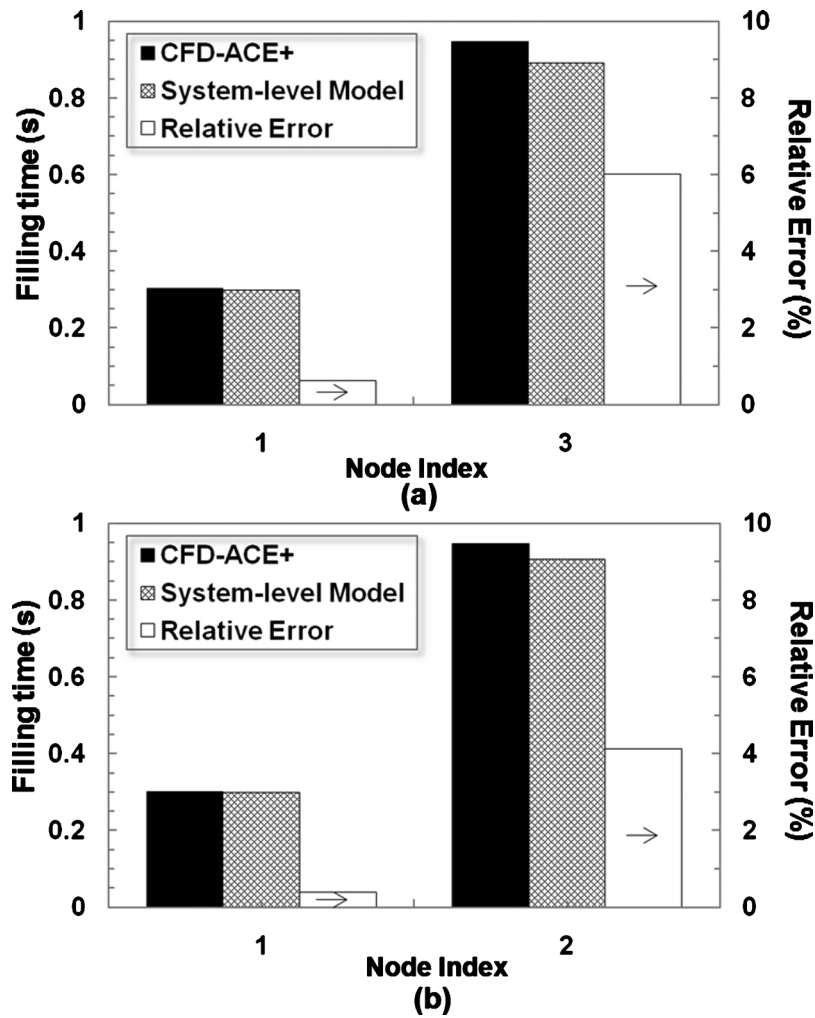


FIG. 9. The filling time of the nodes: (a) $\theta=70^\circ$, (b) $\theta=110^\circ$, and the associated relative errors.

B. Liquid filling in microfluidic multiplexer

The flow multiplexer is a widely used structure to split the sample into multiple streams for high-throughput analysis and passive flow control in microfluidic networks.⁹ To validate its simulation capability for complex microfluidic network, our system-level model was used to investigate the liquid filling process in a two-tier microfluidic multiplexer (involving four outlets) and compared against CFD-ACE+ analysis. The physical model of the microfluidic multiplexer and the corresponding schematic representation were shown in Figs. 1(a) and 1(b). The widths of all channels are $100\ \mu\text{m}$, except for the channel e_3 ($50\ \mu\text{m}$), and the channel e_{15} is ($200\ \mu\text{m}$) to incorporate abrupt shapes and unequal channel width into the complex network and manifest the generality of our system-level simulation. The contact angle is $\theta=110^\circ$ and the inlet flow rate is $0.2\ \text{m/s}$. In our simulations, both 2D (i.e., $H \gg W$ in Fig. 2) and 3D ($H=100\ \mu\text{m}$) are considered.

The comparison of the filling time at different nodes between the CFD-ACE+ and our system-level model is shown in Fig. 12. Both results match very well with the relative error of less than 4% in 2D and 3D cases. The results show that the arrival time to the outlet nodes N_{14} and N_{15} are the longest (0.49 and 0.42 s in the 2D and 3D) and are approximately 30%–60% more than the other two outlet nodes (N_{16} and N_{17}). Furthermore, the asymmetric liquid filling behavior due to

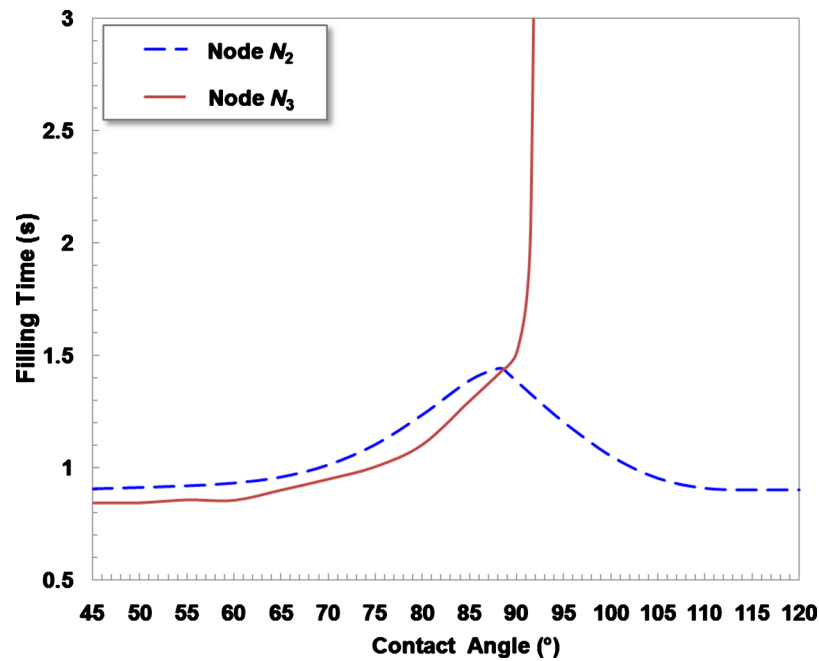


FIG. 10. The filling time of nodes N_2 and N_3 for different contact angles.

unequal branch channel widths in the 2D case is more noticeable than the 3D case due to the introduction of the surface tension force in the third dimension (e.g., comparing the difference in filling times between N_5 and N_7 in both cases, i.e., $\Delta t = t_{N_5} - t_{N_7}$).

The comparison of the computational costs between CFD-ACE+ and the system-level model is summarized in Table II. In the 2D case, 42 900 s (11 h, 55 min) and 0.235 s are needed for CFD-ACE+ and the system-level simulation, respectively, yielding an $\sim 180\,000X$ speedup. In the 3D case, 864 000 s (about 10 days) are required for CFD-ACE+ and only 0.203 s for the system-level simulation, where a salient speedup of 4 200 000X is achieved. Note that the filling time of the whole network in the 2D simulation is larger than that in the 3D simulation (0.5 s versus 0.42 s), leading to slightly longer time of the system-level analysis (0.235 s versus 0.203 s). In addition, simulation involving symmetric branch channel configurations was also carried out, and similar results were observed (data not shown).

VI. CONCLUSION

We have developed a system-level model and simulation framework to investigate the liquid filling process in complex microfluidic networks. The complex microfluidic network is represented as a collection of commonly used components, such as reservoirs, microchannels, and junctions with relatively simple geometries. Dynamic models based on the momentum equation and the principle of mass conservation are developed to track the liquid filling front in such components. The components are then assembled according to their spatial layout and operating rationale to achieve a rapid system-level model, yielding a set of DAEs. The system-level model is then temporally integrated to obtain key information associated with the liquid filling process, including the pressure distribution and liquid front propagation (i.e., the arrival time, speed, and position).

Our model is validated by comparing against the high-fidelity computational tool, CFD-ACE+, in terms of the transient evolution of the liquid filling in a variety of microfluidic constructs (including symmetric branch channels with various junction shapes, asymmetric branch channels, and abrupt-shaped channel structures) and complex microfluidic networks (i.e., multiplexer). Our system-level model demonstrates order-of-magnitude speedup (30 000X–

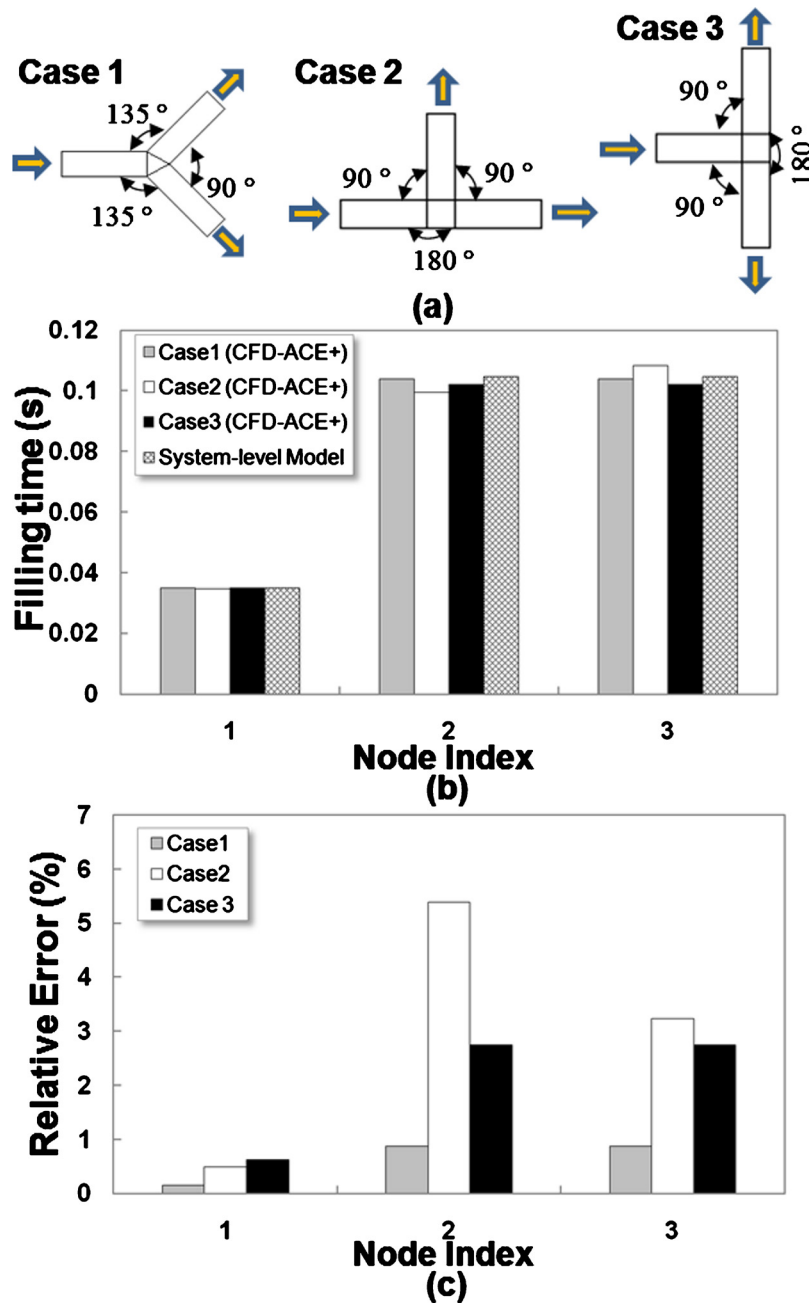


FIG. 11. (a) Y-junction channel with three sets of branch angles and (b) the filling time at the nodes. (c) The relative error between system-level model and CFD-ACE+.

4 000 000X) over the high-fidelity numerical analysis along with good agreement (relative error of less than 7%). The parametric analysis in various microfluidic structures provides several key findings that can be exploited for practical chip design:

- (1) The branch sizes and contact angles have significant impacts on liquid filling. Liquid prefers to enter wide hydrophobic channels or narrow hydrophilic channels. Therefore, the sizes or wettability of channels can be designed to manipulate sample transport and facilitate homogeneous liquid filling, if desired.
- (2) Depending on the application, the local variations in geometries (e.g., asymmetric shapes) or

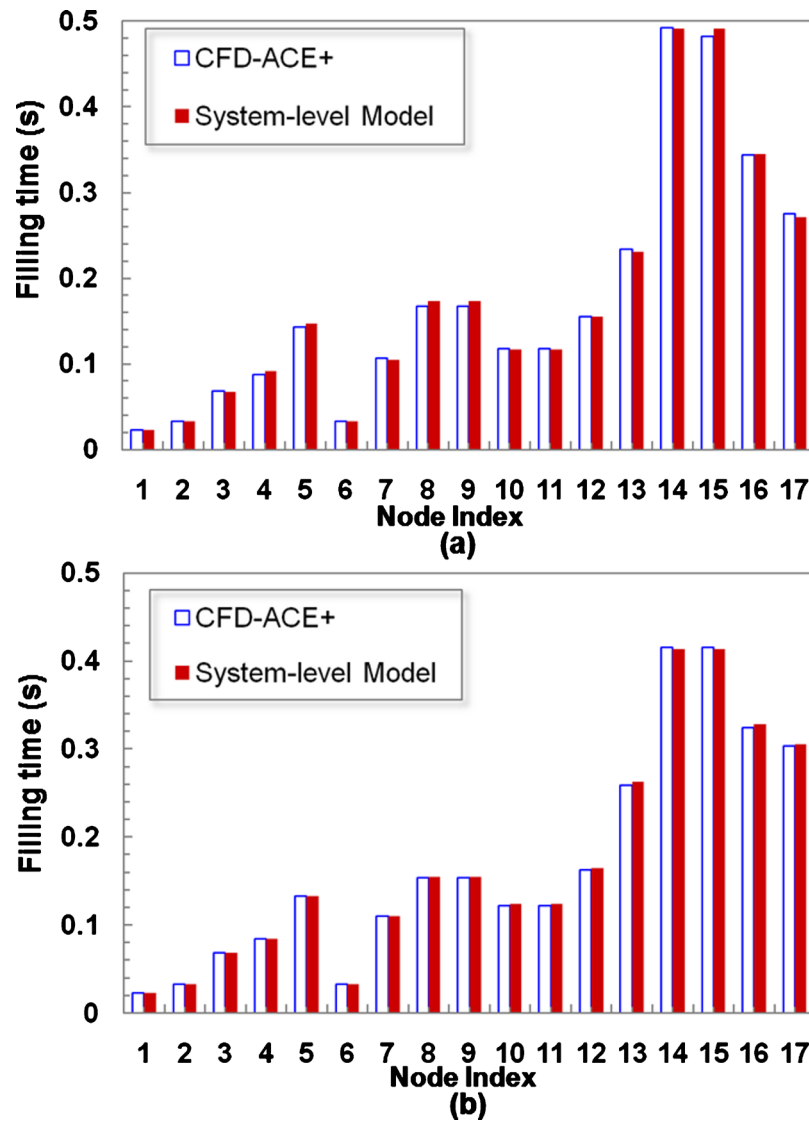


FIG. 12. The filling time at the nodes: (a) 2D channel network and (b) 3D channel network.

surface properties can be exploited to precisely manipulate the liquid filling temporally and spatially. In this regard, a simplified 2D analysis may give rise to large design errors.

- (3) The filling process is virtually independent of the branch angles in microfluidic networks.

Our findings clearly establish the utility of our models and simulation methodology for a fast, reliable analysis of liquid filling to guide the design optimization of complex microfluidic networks. It should be pointed out that the complex, nonideal filling scenarios, such as the precursor

TABLE II. Computational cost of CFD-ACE+ and the system-level model.

	2D	3D
CFD-ACE+	42 900 s (11 h, 55 min)	864 000 s (10 days)
System-level model	0.235 s	0.203 s
Speedup	182 553	4 214 634

films, uncertainty due to surfactants or roughness, and wetting along junctions (e.g., bonding between top and side walls), etc., cannot be taken into account by our system-level models (or even by the high-fidelity numerical model). Future efforts to improve the existing simulation capability will focus on two aspects: model extension to account for dynamics of the isolated gas phase (such as air bubble trapping and propagation) and integration of the model with our system-level microfluidic design tool—Pharos.²⁴

ACKNOWLEDGMENTS

This research was sponsored by NIH/NHGRI under Grant No. 5R44HG004290-03.

- ¹D. Reyes, D. Iossifidis, P. Auroux, and A. Manz, *Anal. Chem.* **74**, 2623 (2002).
- ²A. Auroux, D. Iossifidis, D. Reyes, and A. Manz, *Anal. Chem.* **74**, 2637 (2002).
- ³S. Krishnamoorthy, A. S. Bedekar, J. J. Feng, and S. Sundaram, *J. Assoc. Lab. Autom.* **11**, 118 (2006).
- ⁴V. B. Makhijani, A. J. Reich, A. Puntambekar, C. Hong, and C. Ahn, Technical Proceedings, Fourth International Conference on Modeling and Simulation of Microsystems, Cambridge, MA, 2001, pp. 266–269.
- ⁵J. Zeng, On modeling of capillary filling, http://www.covantor.com/pdfs/on_modeling_of_capillary_filling.pdf (2007).
- ⁶D. S. Kim, K.-C. Lee, T. H. Kwon, and S. S. Lee, *J. Micromech. Microeng.* **12**, 236 (2002).
- ⁷F. G. Tseng, I. D. Yang, K. H. Lin, K. T. Ma, M. C. Lu, Y. T. Tseng, and C. C. Chieng, *Sens. Actuators, A* **97**, 131 (2002).
- ⁸D. Chakraborty, R. A. Gorkin, L. Kulinsky, M. Madou, and S. Chakraborty, *J. Appl. Phys.* **105**, 084904 (2009).
- ⁹C. Ahn, A. Puntambekar, S. Lee, H. Cho, and C. Hong, in *Micro Total Analysis Systems*, edited by A. van den Berg, W. Olthuis, and P. Bergveld (Kluwer, Dordrecht, 2000), pp. 205–209.
- ¹⁰C. H. Ahn, *Proc. IEEE* **92**, 154 (2004).
- ¹¹J.-W. Puntambekar, *Lab Chip* **2**, 213 (2002).
- ¹²H. Q. Yang and A. J. Przekwas, Technical Proceedings of International Conference on Modeling and Simulation of Microsystems, San Juan, Puerto Rico, 1998, pp. 498–505.
- ¹³A. N. Chatterjee and N. R. Aluru, *J. Microelectromech. Syst.* **14**, 81 (2005).
- ¹⁴Y. Wang, A. S. Bedekar, S. Krishnamoorthy, S. S. Siddhaye, and S. Sundaram, NSTI Nanotechnology Conference and Trade Show, Boston, MA, 2006, pp. 546–549.
- ¹⁵Y. Wang, A. S. Bedekar, S. Krishnamoorthy, S. S. Siddhaye, and S. Sundaram, *Microfluid. Nanofluid.* **3**, 307 (2007).
- ¹⁶N. Treise, *Lab Chip* **5**, 285 (2005).
- ¹⁷F. M. White, *Viscous Fluid Flow* (McGraw-Hill, New York, 1991).
- ¹⁸J. Siegrist, M. Amasia, N. Singh, D. Banerjee, and M. Madou, *Lab Chip* **10**, 876 (2010).
- ¹⁹J. J. Chen, W. Z. Liu, J. D. Lin, and J. W. Wu, *Sens. Actuators, A* **132**, 597 (2006).
- ²⁰<http://www.esi-cfd.com/content/blogcategory/82/106/>.
- ²¹X. Mao, S. Yang, and J. Zahn, Proceedings of the ASME-IMECE, Chicago, IL, 2006.
- ²²A. S. Yang, J. C. Yang, and M. C. Hong, *J. Micromech. Microeng.* **16**, 180 (2006).
- ²³J. M. Lai, J. D. Lin, and K. Linliu, *J. Micro/Nanolith. MEMS MOEMS* **9**, 033010 (2010).
- ²⁴A. S. Bedekar, Y. Wang, S. S. Siddhaye, S. Krishnamoorthy, and S. F. Malin, *Clin. Chem.* **53**, 2023 (2007).